Vertically emitting annular Bragg lasers using polymer epitaxial transfer

William M. J. Green,[a] Jacob Scheuer, Guy DeRose, and Amnon Yariv
Departments of Electrical Engineering and Applied Physics, California Institute of Technology, 1200 East California Boulevard, M/C 136-93, Pasadena, California 91125

(Received 24 May 2004; accepted 23 August 2004)

Fabrication of a planar semiconductor microcavity, composed of cylindrical Bragg reflectors surrounding a radial defect, is demonstrated. A versatile polymer bonding process is used to transfer active InGaAsP resonators to a low-index transfer substrate. Vertical emission of in-plane modes lasing at telecom wavelengths is observed under pulsed optical excitation with a submilliwatt threshold. © *2004 American Institute of Physics*. [DOI: 10.1063/1.1807970]

Integrated circular (ring and disk) microresonator-based devices have been studied extensively as key elements within optical communication systems. Numerous active and passive devices, including modulators,[1,2] laser sources,[3,4] all-optical switches,[5,6] channel drop filters,[7,8] and dispersion compensators[9] have been proposed and demonstrated. Interest in such microresonators has recently spread to the field of biosensing,[10,11] making use of the fact that the whispering gallery modes[12,13] are sensitive to subtle environmental changes, via evanescent probing of the immediate surroundings.

Recently, a new ring cavity geometry, based on optimally designed cylindrical Bragg reflectors surrounding a radial defect, was proposed.[14,15] Resonators of this class, known as annular Bragg resonators (ABRs), are designed to support azimuthally propagating modes, with energy concentrated within the defect region by radial Bragg reflection. Optical modes with an electric field having the form $\mathbf{E}(r,\phi,z)=\mathbf{E}(r,z)e^{im\phi}$ have been analyzed using several techniques, including conformal transformation, a transfer matrix approach, coupled mode theory, and finite-difference time-domain simulations. ABR devices are of great interest for their superior sensitivity in biological and chemical sensing applications when compared to conventional total internal reflection (TIR) based resonators.[16] This letter describes the fabrication and experimental demonstration of laser action in a semiconductor annular Bragg resonator.

Annular Bragg resonators with high contrast Bragg reflectors were realized in active semiconductor material. The semiconductor medium consisted of a 250-nm-thick InGaAsP layer ($n\approx 3.35$ at $\lambda=1.55$ μm) on top of an InP substrate. The InGaAsP layer included six 75-Å-wide compressively strained InGaAsP quantum wells positioned at the center, with peak photoluminescence occurring at 1559 nm. Epitaxial layers were grown by MOCVD.

The ABR fabrication process, illustrated in Fig. 1, proceeded as follows. First, a SiO_2 etch mask layer was deposited by PECVD. A layer of PMMA electron beam resist was then applied by spin-coating. The desired ABR geometry was then defined using a Leica Microsystems EBPG 5000+ direct electron beam writer operating at 100 kV. After development, the PMMA patterns were transferred into the SiO_2 etch mask layer by inductively coupled plasma reactive ion etching (ICP-RIE) using C_4F_8 plasma. The remaining PMMA was removed with a gentle isotropic O_2 plasma step. The SiO_2 then served as a hard mask for pattern transfer into the active InGaAsP layer, using an ICP-RIE etch employing HI/Ar chemistry.[17] The patterns were etched to a depth of ~325 nm. The remaining SiO_2 hard mask was then stripped in a buffered hydrofluoric acid solution. A scanning electron microscope (SEM) image of an ABR device at this stage is shown in Fig. 2(a). To achieve strong vertical confinement, the InGaAsP membrane must be clad by low-index material both above and below. An epitaxial layer transfer technique,[18] using an UV-curable optical adhesive (Norland Products NOA 73, $n\approx 1.54$ at $\lambda=1.55$ μm), was adopted to flip-bond the patterned semiconductor sample to a transparent sapphire substrate. Subsequently, the InP substrate was removed by mechanical polishing and selective wet chemical etching, leaving the 250-nm-thick patterned InGaAsP membrane embedded in the cured adhesive. Finally, the adhesive filling the trenches was removed with an isotropic NF_3/O_2 ICP-RIE etch. A magnified view of several transferred annu-

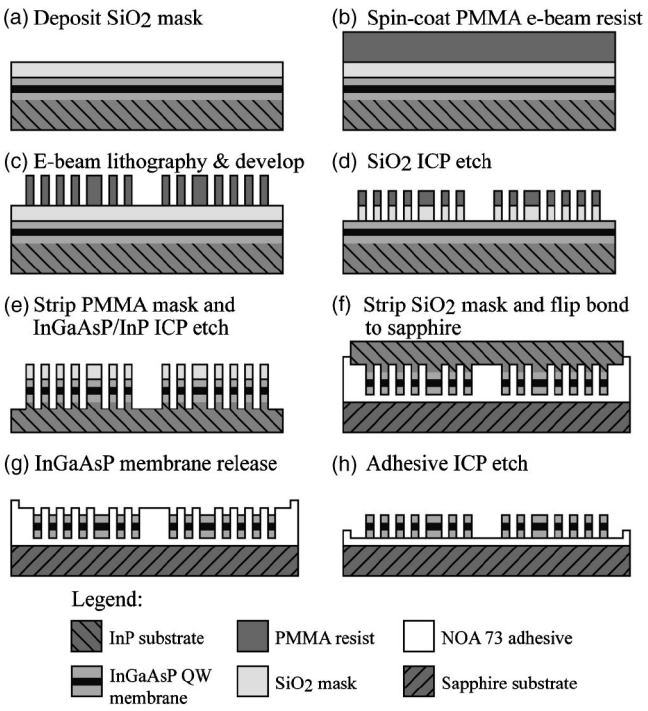

FIG. 1. Flow diagram for annular Bragg resonator fabrication and polymer bonding process. The dark region in the middle of the InGaAsP QW membrane is intended to represent the location of the quantum wells.

[a]Electronic mail: wgreen@caltech.edu

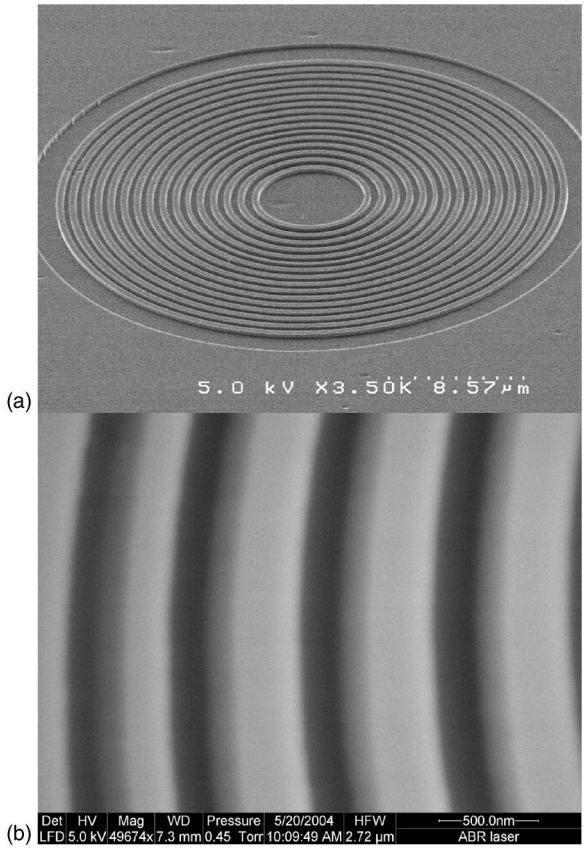

FIG. 2. Scanning electron microscope images of ABR structure tested. (a) Taken after HI/Ar ICP-RIE step, and SiO_2 mask removal. The radial defect is the sixth ring from the center. (b) Magnified image of semiconductor rings, taken after epitaxial transfer process and optical adhesive etch. Brighter regions are the top and side surfaces of the semiconductor rings, dark regions are the trenches from which the adhesive was removed. The HI/Ar etch process results in very smooth and vertical sidewalls.

lar rings, taken after adhesive removal, is shown in Fig. 2(b). Comparison of the two SEM images shows that exposure to the NF_3/O_2 plasma generated no additional roughness on the semiconductor surfaces.

While Bragg reflectors in Cartesian coordinates require gratings with a constant pitch,[19] it has been shown that the optimal cylindrical Bragg reflector requires a "chirped" grating, in which the grating pitch changes as a function of radius.[14] Since optical emission and gain from the compressively strained quantum wells favor TE-polarized electric fields,[20] the ABR devices fabricated used gratings designed for this polarization. In order to simplify the design calculations, an effective index $n_{\text{eff}}=2.8$ (found with a numerical mode solver) was used for the TE-polarized slab mode in the transferred InGaAsP membrane. The Bragg reflectors were of mixed order, with second-order high-index and first-order low-index layers, and were designed for reflection at a center wavelength $\lambda=1550$ nm. The grating pitch was chirped from 0.91 to 0.81 μm from the inner to the outer perimeter. The width of the high-index semiconductor defect was 0.28 μm, chosen for a first-order defect, and the defect radius was 7.72 μm. The Bragg reflectors were composed of five periods to the inside of the radial defect, and ten periods to the outside.

A resonator of the above-mentioned design was pumped by pulsed optical excitation, using a mode-locked Ti:sapphire laser emitting ~100 fs full width at half maximum

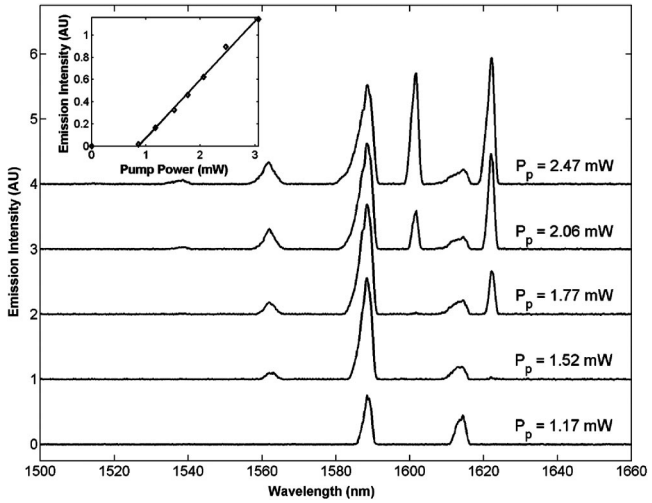

FIG. 3. Optical spectra collected from lasing ABR cavity. Spectra are vertically offset to illustrate effects of increasing pump power. Inset: Integrated ABR emission vs pump power, showing laser threshold of ~860 μW.

pulses at a repetition rate of 78 MHz, with a center wavelength of $\lambda_p=890$ nm. The pump beam was incident normal to the plane of the ABR devices, and focused through the transparent sapphire substrate with a $50\times$(N.A.$=0.42$) microscope objective. Owing to the mixed-order design, the radial component of a wave resonant with the grating completes a full optical cycle between successive grating "periods." Thus, light diffracted vertically from consecutive periods has phase differences of 2π and therefore interferes constructively.[21] The vertically emitted photoluminescence (PL) signal was collected from the side opposite to the pump, using a $20\times$(N.A.$=0.42$) microscope objective. The collected PL was then focused into a multimode optical fiber and fed into an optical spectrum analyzer. Measurements were performed at room temperature.

Emission spectra obtained under several pump intensities are illustrated in Fig. 3, showing multiple lasing modes. The wavelength resolution was 1 nm. Evidence for observation of laser action from this device is given by a clear threshold occurring at ~860 μW, as shown in the inset L–L curve. The pump spot was defocused to a diameter of ~16 μm and centered over the resonator, to ensure even illumination of the radial defect. Under these conditions, two distinct groups of lasing modes were observed. At low pump power ($P_p=1.17$ mW, $P_p=1.52$ mW), resonances at $\lambda_1=1588.7$ nm, $\lambda_2=1614.0$ nm, and $\lambda_3=1562.6$ nm, dominated the spectrum. The FSR of this first group of modes was ~25.5 nm. At an increased pump power of 1.77 mW, an additional mode at $\lambda_4=1622.2$ nm appeared, and at $P_p=2.06$ mW, a mode at $\lambda_5=1601.4$ nm appeared. These new modes were attributed to a second group, owing to their narrower linewidth and smaller FSR of ~20.8 nm. Further increase in pump intensity resulted in increased emission from this second group of modes, with emission from the first group showing saturation. A weak feature at $\lambda_6=1538.0$ nm, belonging to the first group, appeared at the highest pump powers. Linewidth measurements taken from below threshold PL spectra reveal Q factors up to 1000.

In the vertical emission measurement configuration used here, the two distinct groups of lasing modes exhibited different polarization characteristics. The modes of the first group were circularly polarized while the polarization state

of these modes belonging to the second group was slightly elliptical. We attribute the slight deviation of the polarization state of these modes from the expected circular polarization, to fabrication errors that broke the radial symmetry of the device.

The dependence of the vertical diffraction angle in air upon the modal azimuthal number m influences the collection of emitted light.[22] Due to the finite numerical aperture of the collection optics, only modes with $m \leqslant 26$ will be collected efficiently. While the semiconductor rings in the mixed-order Bragg reflectors are wide enough ($\sim 0.43\ \mu$m) to support a transverse guided mode, the observed spectral features in Fig. 3 cannot be attributed TIR-guided whispering gallery modes (WGMs). Since WGMs of the individual semiconductor rings are expected to have $38 \leqslant m \leqslant 176$ (assuming $m\lambda \approx 2\pi R n_{\text{eff}}$, R=ring radius), the collected emission can be attributed to Bragg-guided low-order azimuthal modes, i.e., modes localized within the ABR radial defect. Infrared images of the near-field luminescence profile indicated that the lasing pattern consisted of two concentric rings, one of them located in the internal grating region while the other was localized in the radial defect.

The multiple modes belonging to each group are likely to posses a similar radial profile, with consecutive azimuthal numbers (m, $m+1$, $m+2$, etc.). Dissimilarities in the threshold and FSR between the two groups of modes suggest they may possess slightly different radial profiles and/or different overlap with the pump spot. Differences such as these could arise from multiple transverse modes within the radial defect, and/or localization at different radii within the ABR structure. Comparison of experimental spectra with the results of numerical simulations can provide further insight into the spatial distribution of ABR modes, and will be the subject of a subsequent publication.[23]

In summary, laser oscillation in semiconductor annular Bragg resonators was demonstrated under pulsed optical excitation with a threshold of $\sim 860\ \mu$W. Devices were fabricated within a thin InGaAsP quantum well membrane by electron beam lithography and reactive ion etching, along with a polymer epitaxial transfer technique. The technique demonstrated provides a simple means of integrating functional, compact ABR devices within optical communication or biosensor systems.

The authors would like to thank Dr. Axel Scherer and Dr. Oskar Painter for providing access to their fabrication facilities. George Paloczi and Dr. Reginald Lee are also acknowledged for fruitful discussions. This work was supported by the National Science Foundation and DARPA.

[1] A. Yariv, IEEE Photonics Technol. Lett. **14**, 483 (2002).
[2] P. Rabiei, W. H. Steier, C. Zhang, and L. R. Dalton, J. Lightwave Technol. **20**, 1968 (2002).
[3] J. P. Hohimer, D. C. Craft, G. R. Hadley, G. A. Vawter, and M. E. Warren, Appl. Phys. Lett. **59**, 3360 (1991).
[4] S. J. Choi, K. Djordjev, S. J. Choi, and P. D. Dapkus, IEEE Photonics Technol. Lett. **15**, 1330 (2003).
[5] V. Van, T. A. Ibrahim, K. Ritter, P. P. Absil, F. G. Johnson, R. Grover, J. Goldhar, and P.-T. Ho, IEEE Photonics Technol. Lett. **14**, 74 (2002).
[6] J. E. Heebner, N. N. Lepeshkin, A. Schweinsberg, G. W. Wicks, and R. W. Boyd, Opt. Lett. **29**, 769 (2004).
[7] B. E. Little, J. S. Foresi, G. Steinmeyer, E. R. Thoen, S. T. Chu, H. A. Haus, E. P. Ippen, L. C. Kimerling, and W. Greene, IEEE Photonics Technol. Lett. **10**, 549 (1998).
[8] D. G. Rabus and M. Hamacher, IEEE Photonics Technol. Lett. **13**, 812 (2001).
[9] C. K. Madsen and J. H. Zhao, *Optical Filter Design and Analysis: A Signal Processing Approach* (Wiley-Interscience, New York, 1999).
[10] R. W. Boyd and J. E. Heebner, Appl. Opt. **40**, 5742 (2001).
[11] S. Blair and Y. Chen, Appl. Opt. **40**, 570 (2001).
[12] L. Rayleigh, in *Scientific Papers* (Cambridge University, Cambridge, UK, 1912), Vol. 5, 617 pp.
[13] S. L. McCall, A. F. J. Levi, R. E. Slusher, S. J. Pearton, and R. A. Logan, Appl. Phys. Lett. **60**, 289 (1992).
[14] J. Scheuer and A. Yariv, J. Opt. Soc. Am. B **20**, 2285 (2003).
[15] J. Scheuer and A. Yariv, IEEE J. Quantum Electron. **39**, 1555 (2003).
[16] J. Scheuer, W. M. J. Green, G. DeRose, and A. Yariv, presented at the Photonics West Conference on Laser Resonators and Beam Control VIII, San Jose, CA, 2004, p. 183.
[17] S. J. Pearton, U. K. Chakrabarti, A. Katz, F. Ren, and T. R. Fullowan, Appl. Phys. Lett. **60**, 838 (1992).
[18] S. R. Sakamoto, C. Ozturk, Y. T. Byun, J. Ko, and N. Dagli, IEEE Photonics Technol. Lett. **10**, 985 (1998).
[19] A. Yariv, *Optical Electronics in Modern Communications*, 5th ed. (Oxford University Press, New York, 1997).
[20] L. A. Coldren and S. W. Corzine, *Diode Lasers and Photonic Integrated Circuits* (Wiley-Interscience, New York, 1995).
[21] A. Shaw, B. Roycroft, J. Hegarty, D. Labilloy, H. Benisty, C. Weisbuch, T. F. Krauss, C. J. M. Smith, R. Stanley, R. Houdre, and U. Oesterle, Appl. Phys. Lett. **75**, 3051 (1999).
[22] Azimuthally propagating modes in the ABR structure contain $\exp(im\phi)$ dependence. Upon circulation around a loop of radius r, the mode advances in phase by $\exp(ik_\phi L)=\exp(i2k_\phi \pi r)=\exp(i2m\pi)$, resulting in $k_\phi = m/r$. Using Snell's law to estimate the air diffraction angle θ_0 in the azimuthal direction, one finds $\sin\theta_0 = k_\phi/k_0 = \lambda_0 m/2\pi r$, where $k_0 = 2\pi/\lambda_0$. At $\lambda_0 = 1.55\ \mu$m, light enters the collection optics ($\sin\theta_0 \leqslant 0.42$) only up to $m=26$ at $r=16\ \mu$m, corresponding to the outer radius of the ABR device.
[23] J. Scheuer, W. M. J. Green, G. DeRose, and A. Yariv, Opt. Lett. **29**, 2641 (2004).